

1 **Evolution of southern Benguela Upwelling System and Agulhas Leakage over the last 3.5 Ma**

2 Benjamin Petrick<sup>1,2</sup>; Erin L. McClymont<sup>3</sup>; Kate Littler<sup>4</sup>; Antoni Rosell-Melé<sup>5,6</sup>; Matthew O. Clarkson<sup>7</sup>;  
3 Mark Maslin<sup>8</sup>, Ursula Röhl<sup>9</sup>; Amelia E. Shevenell<sup>8,10</sup>; Richard D Pancost<sup>11</sup>

4 1 Max Planck Institute of Chemistry, Climate Geochemistry Department, Hahn-Meitner-Weg 1,

5 55128 Mainz Germany

6 2. Department of Geography, Newcastle University,

7 3 Department of Geography, Durham University, South Road, Durham, DH1 3LE, U.K.

8 4 Camborne School of Mines & Environment and Sustainability Institute University of Exeter

9 5 Institute of Environmental Science and Technology, Autonomous University of Barcelona, Campus  
10 de la UAB 08193 Bellaterra (Cerdanyola del Vallès), Barcelona, Spain

11 6 Institució Catalana de Recerca i Estudis Avançats, 08010 Barcelona, Catalonia, Spain.

12 7 Institute of Geochemistry and Petrology, Department of Earth Sciences, ETH, 8092, Zurich,  
13 Switzerland

14 8. Department of Geography University College London, Pearson Building, Gower Street, London,  
15 WC1E 6BT

16 9. MARUM – Center for Marine Environmental Sciences, University of Bremen, Leobener Str. 8,  
17 28359 Bremen, Germany

18 10.College of Marine Science, University of South Florida, St. Petersburg, FL 33701, USA

19 11. University of Bristol School of Chemistry, Cantock's Close, BS8 1TS, Bristol UK

20 **Abstract**

21 The southeast Atlantic Ocean is dominated by two major oceanic systems: the Agulhas  
22 Leakage, which is important for transferring warm salty water from the Indian Ocean to the Atlantic  
23 Ocean and the Benguela Upwelling System, one of the world's most productive coastal upwelling

24 cells. Here, we present a multi-proxy record of marine sediments from ODP Site 1087. We  
25 reconstruct sea surface temperatures ( $U_{37}^K$  and  $TEX_{86}$  indices), marine primary productivity (total  
26 chlorin and alkenone mass accumulation rates), and terrestrial inputs derived from southern Africa  
27 (Ti/Al and Ca/Ti via XRF scanning) to understand the evolution of Agulhas Leakage and the Benguela  
28 Upwelling System since the late Pliocene. In the late Pliocene and early Pleistocene, ODP Site 1087  
29 was situated within the Benguela Upwelling System, which was displaced southwards relative to  
30 present. We recognize a series of events in the proxy records at 3.3, 3.0, 2.2, 1.5, 0.9 and 0.6 Ma,  
31 which are interpreted to reflect a combination of changes in the location of major global wind and  
32 oceanic systems and local variations in the strength and/or position of the winds, which influences  
33 nutrient availability. Although there is a temporary SST cooling observed around the initiation of  
34 Northern Hemisphere glaciation (iNHG), proxy records from ODP Site 1087 show no clear climatic  
35 transition around 2.7 Ma. This observation is significant because it has been previously suggested  
36 there should be a change in the location and/or strength of upwelling associated with this climate  
37 transition. Rather, the main shift at ODP Site 1087 occurs at ca. 0.9 Ma, associated with the early  
38 mid-Pleistocene transition (EMPT), when Agulhas Leakage replaces an upwelling-dominated regime.  
39 This observation raises the possibility that reorganisation of southeast Atlantic Ocean circulation  
40 towards modern conditions was tightly linked to the EMPT, but not to earlier climate transitions.

41

## 42 **1.1 Introduction**

43 Over the last 3.5 Ma, Earth's climate transitioned from warmer climates of the Pliocene to  
44 cooler Pleistocene climates (Haug et al., 2005; McClymont et al., 2013). Two of the biggest climate  
45 transitions were the intensification of Northern Hemisphere glaciation (iNHG; 3.0 and 1.5 Ma), when  
46 Northern Hemisphere ice sheets expanded and the oceans cooled (Haug et al., 2005), and the early  
47 mid-Pleistocene transition (EMPT; 1.2 and 0.6 Ma), when glacial-interglacial cycles shifted to a quasi  
48 100ka period (Chalk et al., 2017; Maslin and Brierley, 2015; McClymont et al., 2013). Shifts in the

49 location and intensity of the major ocean upwelling cells are thought play an important role in global  
50 climate during the Plio-Pleistocene (Lawrence et al., 2013; März et al., 2013). For example, the  
51 equatorward migration of the major wind cells between 3.3 and 1.0 Ma resulted in a concomitant  
52 shift of the subtropical and polar upwelling zones and increased global carbonate production,  
53 affecting the global atmosphere-ocean CO<sub>2</sub> exchange (Lawrence et al., 2013; Martínez-García et al.,  
54 2011). Additionally, models show that cooler sea surface temperatures (SSTs) in upwelling zones can  
55 affect mean global atmospheric temperatures, as upwelling cells supply cooler deeper waters to the  
56 surface ocean (Barreiro et al., 2005).

57 Debate exists about the precise timing of upwelling shifts during the Plio-Pleistocene and  
58 whether the changes in location and focus of the different upwelling systems reflect local, rather  
59 than global, factors (Dekens et al., 2007; Lawrence et al., 2013; Rosell-Melé et al., 2014). Lawrence  
60 et al. (2013) proposed that between 3.3 and 2.5 Ma, the build-up of ice sheets in the Northern  
61 Hemisphere caused the westerlies to shift equatorward and the Hadley Cells to contract, shifting the  
62 location of the trade winds. These authors propose that the shift in the wind fields resulted in  
63 cooling and increased productivity in major North and South Atlantic Ocean upwelling cells. Others  
64 have suggested, based on SST cooling around 3.3 Ma (Dekens et al., 2007), that upwelling cells were  
65 invigorated before the intensification of glacial stages at 2.7 Ma (MIS 96-100) (Haug et al., 2005).  
66 Later upwelling intensification in the Benguela system around 2 Ma has been inferred from SST  
67 cooling and increased productivity (Etourneau et al., 2010, 2009). Thus, it remains unclear whether  
68 changes in upwelling activity across the Plio-Pleistocene transition were influenced by global climate  
69 transitions or occurred independently.

70 ODP Site 1087 (31°28'S, 15°19'E; 1374 m water depth) is located near the southern cell of  
71 the modern Benguela Upwelling System (Figure 1). Foraminiferal assemblages, SST reconstructions,  
72 and marine organic matter inputs indicate that ODP Site 1087 was influenced by the Benguela  
73 Upwelling System during the Pliocene (3.5–3.0 Ma; Petrick et al., 2015a). However, during the mid to

74 late Pleistocene (0–0.6 Ma), foraminiferal assemblage, SST, and salinity records indicate that the site  
75 was primarily influenced by Indian Ocean waters via the Agulhas Leakage, with evidence of  
76 upwelling limited to a few glacial periods (Caley et al., 2014, 2012; McClymont et al., 2005; Petrick et  
77 al., 2015b). What remains unclear is the nature and timing of the transition from an upwelling-  
78 dominated to a leakage-dominated regime, and whether this shift occurred as part of the iNHG or  
79 the EMPT. The timing of this transition may have important climatic implications, as intensification  
80 of Agulhas leakage enhances heat and salt transfer into the Southeast Atlantic Ocean, which may  
81 influence the strength of the AMOC (Biajoch et al., 2008). The continuous Plio-Pleistocene sediment  
82 sequence from ODP Site 1087 provides an ideal archive from which to reconstruct the evolution of  
83 the southern Benguela upwelling and Agulhas leakage systems over the Plio-Pleistocene.

84

## 85 **1.2 Oceanographic Setting and paleoclimate history**

86 The Benguela Upwelling System is a key oceanographic upwelling region that developed  
87 around the mid-Miocene (Diester-Haass, 1988). The Benguela upwelling is one of the few major  
88 temperate upwelling sites in the world. It is an area that is that releases CO<sup>2</sup> and is important for  
89 biological cycling in the ocean (Compton et al., 2009; West et al., 2004). Therefore understating the  
90 history of the system under different climate regimes is important for understanding the effects and  
91 impacts of climate change. It has been proposed that the main focus of the Benguela Upwelling  
92 System has migrated northward from the southern Benguela region to its current location since the  
93 mid-Pliocene (Christensen and Giraudeau, 2002; Petrick et al., 2015a; Rosell-Melé et al., 2014).  
94 Changes in temperature and productivity have been well documented in the northern (ODP Sites  
95 1082 and 1081; Figure 1) and central Benguela upwelling cells (ODP Site 1084) over the last 3.5 Ma  
96 (Etourneau et al., 2009; Marlow et al., 2000; Rosell-Melé et al., 2014). Initial cooling began gradually  
97 in the northern and central cells started around 3.5 Ma, with a 0–1°C gradient from the northern to  
98 central upwelling cells (Rosell-Melé et al., 2014). Around 3.0 Ma, there was an increase in diatom

99 production, marking the Matuyama Diatom Maximum (MDM), in the northern and central Benguela  
100 regions (3.0–2.5 Ma) (Robinson and Meyers, 2002). Around 1.5 Ma, there was major cooling at all  
101 three sites and the development of a 3–4°C gradient between the northern and central cells (Rosell-  
102 Melé et al., 2014). Regional primary productivity was stable until 2.4 Ma, when it increased in the  
103 central cells (Rosell-Melé et al., 2014); productivity increased in the northern cells at 0.6 Ma (Rosell-  
104 Melé et al., 2014). Constriction and northward movement of the Hadley cells since the Pliocene is  
105 hypothesized to have shifting the focus of upwelling equatorward (Etourneau et al., 2010; Rosell-  
106 Melé et al., 2014). More recently, models indicate that tectonic mountain-building in west Africa  
107 may have influenced the position and intensity of the trade winds, resulting in the onset and  
108 northward migration of upwelling since the mid-Miocene (Jung et al., 2014).

109 Presently, sea surface conditions at ODP Site 1087 are influenced by the Agulhas Leakage  
110 (Figure 1) (Gordon et al., 1987; Gordon and Haxby, 1990), which transfers rings of warm and salty  
111 water from the Indian Ocean to the Atlantic Ocean. This is the key way that surface water is  
112 transferred from the Indian Ocean to the Atlantic Ocean. These rings are then advected northwards  
113 and ultimately incorporated into the Atlantic Meridional Overturning circulation (AMOC) (Hall and  
114 Lutjeharms, 2011). Through its impact on salt transfer to the North Atlantic, the intensity of Agulhas  
115 Leakage has been shown to influence the strength of the AMOC over centennial to millennial scale  
116 times (Biaosoch et al., 2008; Knorr and Lohmann, 2003). In climate models, increases in the Agulhas  
117 Leakage are able to restart the thermohaline circulation after a period of shutdown (e.g., in response  
118 inputs of fresh waters to the North Atlantic; Knorr and Lohmann, 2003). Increased Agulhas Leakage  
119 has also been shown to be a prominent feature of deglaciations over the last 1200 kyr (Beal et al.,  
120 2011) and may have prevented an early return to glacial conditions such as during the Younger  
121 Dryas though increasing input of high salinity waters to the source of the Atlantic thermohaline  
122 circulation (Dyez et al., 2014; Marino et al., 2013; Scussolini et al., 2015). Furthermore other studies  
123 have shown that this salt leakage seems to have existed since at least 500ka ( Petrick et al., 2015)

124 Today ODP 1087 does not receive much terrestrial input. The modern day site is on the  
125 edge of the Namibian dust plume(Kienast et al., 2016; Mahowald et al., 2014). Therefore the  
126 amount of dust reaching the site is limited is relatively minor. The Orange River provides a minor  
127 source of riverine input. While the majority of the input from the Orange River occurs far north of  
128 the site some finer partials are incorporated into the turbulent Cape Basin Area (Bluck et al., 2007;  
129 Boebel et al., 2003; Compton and Maake, 2007). These then are transported through out the cape  
130 basin (Boebel et al., 2003). However overall the amount of terrestrial material is low compared to  
131 other sites in the region.

132 In order to track shifts in upwelling strength over the last 3.5 Ma, we applied a multiproxy  
133 approach to sediments from ODP Site 1087 (Figure 1). Two biomarker temperature proxies, the  $U^{K_{37}}$   
134 and  $TEX_{86}$  indices (Müller et al., 1998; Schouten et al., 2002) were used to reconstruct SSTs, which  
135 are sensitive to upwelling strength. Additionally, concentrations of chlorins and alkenones were  
136 determined to assess primary productivity and coccolithophore productivity, respectively (Harris et  
137 al., 1996). Ca/Ti ratios from XRF scanning were used as a proxy of carbonate deposition/preservation  
138 at the site which may relate to changes in productivity. Terrestrial inputs were assessed using Ti/Al  
139 counts, which has been shown for the SE Atlantic to track dust over riverine input (Govin et al.,  
140 2012). For more information about the Interpretation and complications of the proxy signals see the  
141 supplemental data.

142 The  $U^{K_{37}}$ -derived SSTs and alkenone mass accumulation rate (MAR) data for the last 1.5 Ma  
143 are published (McClymont et al., 2005; Petrick et al., 2015a). However, the new data we present  
144 allow a better understanding of: 1) changes in the vertical temperature structure of the upper water  
145 column ( $U^{K_{37}}$ -  $TEX_{86}$ ), which gives an indication of upwelling strength; because research shows that  
146 in Benguela sourced water that SSTs are lower in  $TEX_{86}$  then  $U^{K_{37}}$ . By comparing periods were the  
147 two proxies record different temperature to those where the SSTs are the same we can track the  
148 presence of Upwelling sourced water. 2) changes in terrestrial inputs (Ti/Al) and potential wind-

149 forcing of any upwelling changes; and 3) associated changes in marine productivity (alkenone and  
150 chlorin MAR). These new data are placed in a regional context through comparison to similar  
151 datasets from the northern and central Benguela Upwelling System (ODP Sites 1081, 1082, and  
152 1084; Fig. 1), and from farther south at the sub-tropical front (ODP Site 1090).

## 153 **2. Methods**

154 ODP Site 1087 is located in the SE Atlantic Ocean (Shipboard Scientific Party, 1998) (Figure  
155 1). All of the sediments analysed in this study are from the shipboard-defined lithologic "Unit I",  
156 which is described as a moderately bioturbated olive to olive-grey foraminifera-nannofossil ooze,  
157 with 50-100 cm thick nannofossil oozes in the upper 45 m (Shipboard Scientific Party, 1998). The age  
158 model for the age between 0-1.5 Ma and 3.0-3.5 Ma and sampling strategy are based on  
159 foraminifera oxygen isotope stratigraphies tuned to the LR04  $\delta^{18}\text{O}$  stack (McClymont et al., 2005;  
160 Petrick et al., 2015a, 2015b). We assume linear sedimentation rates between the shipboard age  
161 model tie-points between 1.5-3.0 Ma (Shipboard Scientific Party, 1998). The average sampling  
162 resolution is 5 cm, which translates to a temporal resolution of 3-kyr in the Pliocene and Mid- to  
163 Late-Pleistocene, and 10-kyr in the early Pleistocene.

### 164 **2.1 Biomarker analysis**

165 The biomarkers (alkenones, chlorins, and glycerol dialkyl glycerol tetraethers (GDGTs)) were  
166 extracted from homogenised, freeze-dried sediment using a CEM microwave system with 12 ml of  
167 DCM:MeOH (3:1, v/v). Internal standards were added for quantification (5 $\alpha$ -cholestane,  
168 dotriacontane and tetracontane). The microwave temperature programme heats samples to 70°C  
169 over a 5 minute temperature ramp, holds temperatures at 70°C for 5 minutes, and then cools over  
170 30 minutes (Kornilova and Rosell-Mele, 2003). The supernatant was decanted into vials and dried  
171 under a nitrogen stream. An aliquot was taken for chlorin concentration and TEX<sub>86</sub> analyses and the  
172 remainder was derivatised using N,O- Bis(trimethylsilyl)trifluoroacetamide with trimethylchlorosilane  
173 at 70 °C for 1 hour before alkenone analysis.

174 Alkenones were analysed using a gas chromatograph fitted with a flame-ionisation detector  
175 (GC-FID) and a 30 m HP1-MS capillary column. The injector temperature was held at 300°C and the  
176 detector at 310°C. The oven program is as follows: after injection, hold at 60°C for 1 min, increase to  
177 120°C at 20°C m<sup>-1</sup>, to 310°C at 6°C m<sup>-1</sup>, and hold at 310°C for 30 min. The alkenone abundances were  
178 converted to MAR using linear sedimentation rates and the shipboard dry bulk density  
179 measurements (Shipboard Scientific Party, 1998). The U<sup>K</sup><sub>37'</sub> was calculated using the relative  
180 abundances of the C<sub>37:3</sub> and C<sub>37:2</sub> alkenones (Prahl and Wakeham, 1987), and converted to SSTs using  
181 the Müller et al. (1998) core-top calibration. The error associated with the analytical measurement is  
182 ±0.5°C while the calibration error equates to ±1.0°C (Müller et al., 1998).

183 A subset of samples was selected for TEX<sub>86</sub> analysis, guided by our U<sup>K</sup><sub>37'</sub> results, with the aim  
184 of ensuring a broad spectrum of both warm and cold periods was represented. The GDGT fraction  
185 was re-dissolved in 200 µl of hexane:n-propanol (98.5:1.5, v/v) and an internal standard was added.  
186 The sample and standard filtered through a 0.5 µm PTFE filter. The filtered samples were analysed  
187 by High-Performance Liquid Chromatography Mass Spectrometry (HPLC-MS), using a Dionex P680  
188 HPLC coupled to a Thermo Finnigan TSQ Quantum Discovery Max quadrupole mass spectrometer at  
189 the University of Barcelona Automatica, with an atmospheric pressure chemical ionization (APCI)  
190 interface set in positive mode. The GDGTs were eluted through a Tracer Excel CN column  
191 (Teknokroma) with a length of 20 cm, a diameter of 0.4 cm and a particle size of 3 µm. There was a  
192 guard column on the other end of the set-up. The mobile phase was initially hexane:n-propanol  
193 (98.5:1.5) at a flow of 0.6 mL min<sup>-1</sup>. The proportion of n-propanol was kept constant at 1.5% for 4  
194 minutes, increased gradually to 5% during 11 minutes, increased to 10% for 1 minute, held for 4  
195 minutes, decreased back to 1.5% during 1 minute, and held at these conditions for 9 minutes. The  
196 parameters of the APCI interface were set as follows to generate positive ion spectra: corona  
197 discharge 3 µA, vaporizer temperature 400 °C, sheath gas pressure 49 mTorr, auxiliary gas (N<sub>2</sub>)  
198 pressure 5 mTorr, and capillary temperature 200 °C. A subset of samples was analysed using the  
199 HPLC system at University College London (UCL). The error associated with the analytical



200 measurement is  $\pm 1.0^{\circ}\text{C}$  while the calibration error (BAYSPAR; Tierney and Tingley, 2014) varies  
201 according to geographic location, but on average for this record equates to  $\pm 7.0^{\circ}\text{C}$ .

202 Chlorins were analysed using an HPLC system coupled to a photo-diode array  
203 spectrophotometer. Solvent extracts were dissolved in acetone and injected three times. The PDA  
204 scanned across 350 – 800 nm and absorbance at the wavelengths 410 and 665 nm was quantified.  
205 Sample means of the triplicate measurements are reported here. Analytical variability was  
206 monitored using repeat measurements of a standard and was determined at 0.07 absorbance units  
207 (abs). For all samples, the absorbance at 410 nm or 665 nm was divided by the total dry weight of  
208 the sample to calculate absorbance/g and then converted to mass accumulation rate (MAR) using  
209 the linear sedimentation rates and the shipboard dry bulk density measurements (Zachos et al.,  
210 2004).

211

## 212 **2.2 XRF analysis**

213 Elemental data was collected using an XRF Core Scanner II (AVAATECH Serial No. 2) at the  
214 MARUM, University of Bremen. The reported data here have been acquired by a Canberra X-PIPS  
215 Silicon Drift Detector (SDD; Model SXD 15C-150-500) with 150eV X-ray resolution, the Canberra  
216 Digital Spectrum Analyser DAS 1000, and an Oxford Instruments 50W XTF5011 X-Ray tube with  
217 rhodium (Rh) target material. Elements (Fe, Ca, Ti) were collected at a resolution of 2-cm down-core,  
218 over a 2 cm<sup>2</sup> area with down-core slit size of 10 mm, using generator settings of 10 kV, a current of  
219 0.15 mA, and a sampling time of 20 seconds directly at the split core surface of the archive half. The  
220 split core surface was covered with a 4-micron thin SPEXCerti Prep Ultralene1 foil to avoid  
221 contamination of the XRF measurement unit and desiccation of the sediment. Raw data spectra  
222 were processed by the analysis of X-ray spectra by the Iterative Least square software (WIN AXIL)  
223 package from Canberra Eurisys. Due to previous oversampling, it was impossible to scan the upper  
224 four sections of the core. Additionally, because of the time between the core being taken and the  
225 XRF scanning, it was impossible to normalize the XRF scanning data to the initial shipboard data.

226

## 227 **3. Results**

### 228 **3.1 Sea surface temperature trends**

229 Two separate biomarker indices were used to calculate SSTs: higher resolution data using  
230 the  $U^{K_{37}}$  proxy (from alkenones), and lower resolution data using the  $TEX_{86}$  proxy (from GDGTs). For  
231 more information about the calibrations used see supplemental data. Over the last 3.5 Ma,  $U^{K_{37}}$ -  
232 derived SST values at ODP Site 1087 range between 12 and 24°C (Figures 2 and 3), with an average  
233 of around 18°C. Overall, the SST trends can be summarised as: stable SSTs between 3.5 and 1.7  
234 Ma, 3° C cooling between 1.7 and 0.9 Ma, and 2° C warming SSTs from 0.9 Ma to present (Figures 2  
235 and 3). The coldest SSTs of 12°C occurred around 0.5 Ma (Marine Isotope Stage (MIS) 13). The  
236 highest SST variability (~10°C) across glacial-interglacial timescales occurs after 0.9 Ma.

237 The lower resolution  $TEX_{86}$ -derived SSTs range from 10 to 24°C over the last 3.5 Ma, with an  
238 average of ~16 °C (Figure 2). The SSTs were relatively stable before ~0.9 Ma, after which there is  
239 increased variability in the data and evidence for 2° C warming towards the present. Before 0.9 Ma,  
240 the  $TEX_{86}$ -derived SSTs are cooler than coeval  $U^{K_{37}}$ -derived SSTs by up to 10°C. After 0.9 Ma,  $TEX_{86}$ -  
241 derived SSTs are either similar to, or warmer than, the  $U^{K_{37}}$  -derived SSTs. The difference between  
242 the two temperature proxies indicate that the  $U^{K_{37}}$  temperatures are only cooler after 0.6 Ma  
243 (Figure 2)

### 244 **3.2 Productivity proxies**

245 Three proxies were used to track changes in the primary productivity of the site: 1) chlorin  
246 MAR; 2) alkenone mass accumulation rates (MAR); and 3) Ca/Ti ratios generated from XRF scanning.  
247 Chlorin MARs range between 0.001 and 1.0 g<sup>2</sup> abs cm<sup>-2</sup> kyr<sup>-1</sup> (Figure 3). Between 1.7 and 0.5 Ma,  
248 chlorin MARs are elevated, which contrasts with low values (<0.05 abs cm<sup>-2</sup> kyr<sup>-1</sup>) between 3.0–1.7  
249 Ma. A return to low chlorin MARs for the last 0.4 Ma is recorded after a final high peak in chlorins

250 during MIS 10. Alkenone MAR ranges between 1 and 12  $\mu\text{g cm}^{-2} \text{ kyr}^{-1}$ , with an overall zone of low  
251 amplitude oscillations between 3.0 and 2.5 Ma (Figure 3). After 0.9 Ma, the highest values occur in  
252 MISs 14, 12, 10, and 8. Ca/Ti values range between 100 and 1800 (Figure 4). The lowest values are  
253 around 3.1 Ma; with a slight increase around 3.0 Ma, followed by stable Ca/Ti ratios. Ca/Ti then  
254 increases towards the modern day, starting around 1.6 Ma, with the highest values around 0.4 Ma  
255 although there are no glacial-interglacial trends in the data.

### 256 **3.3 Terrestrial proxy**

257 Ti counts range from 1000 to 8000 counts at ODP Site 1087 (Figure 4). The highest Ti values  
258 are before 3.0 Ma. At 3.0 Ma Ti counts decrease, and then there is a brief increase around 2.5 Ma,  
259 with three large Ti peaks around MIS 96-102. Outside of these periods, Ti remains relatively low (<  
260 2000 counts). There is no clear glacial – interglacial variation in the Ti data.

261

## 262 **4. Discussion**

### 263 **4.1 Climatic and oceanographic variability at ODP Site 1087 from 3.5 to 0.0 Ma**

264 Overall, the Site 1087 records indicate a gradual transition from an upwelling-dominated  
265 record in the Pliocene and early Pleistocene to an Agulhas Leakage-dominated record in the mid to  
266 late Pleistocene (Figures 3; 4). During the late Pliocene (3.5–3.0 Ma), warmer SSTs, higher  
267 productivity, and a 6-7°C offset in the  $\text{TEX}_{86}$ - and  $\text{U}^{\text{K}}_{37}$ '-derived temperatures suggest that more high  
268 nutrient upwelling sourced water reached Site 1087 (Petrick et al., 2015a). A period of lower  
269 productivity and lower Ti counts marks the late Pliocene–early Pleistocene (3.0–2.0 Ma), with less  
270 terrestrial input and mostly stable SSTs. During this interval, there continues to be an offset between  
271  $\text{TEX}_{86}$ - and  $\text{U}^{\text{K}}_{37}$ '-derived temperatures, but this varies between 4 and 11°C, indicating variable  
272 upwelling intensity. The period between 1.5 and 0.6 Ma is characterised by an increase in  
273 productivity, cooler SSTs, and a reduction in the  $\text{TEX}_{86}$ - $\text{U}^{\text{K}}_{37}$ ' temperature offset (Figure 2). Finally, the

274 mid- to late Pleistocene (0.6–0.0 Ma) is defined by warming SSTs, variable productivity with higher  
275 productivity during glacials, and lower terrestrial input (from Ti). These trends, coupled with the  
276 previously published data, indicate that over the last 500 ka there has been increased warm water  
277 input through the Agulhas Leakage during prominent interglacials, punctuated by glacial periods with  
278 high productivity (Petrick et al., 2015b). For a further analysis of the proxies used in making the  
279 reconstruction please see the supplemental material.

280 It has been proposed that tectonic uplift along the Namibian coast since the Pliocene could  
281 have increased upwelling intensity and slowly shifted upwelling cells northward (Jung et al., 2014).  
282 Overall, the data from Site 1087 is broadly consistent with this hypothesis, but this time interval also  
283 includes several known global climate changes, which are hypothesised to have impacted  
284 subtropical upwelling systems. Here, we evaluate the links to other potential forcing mechanisms  
285 driven by Plio-Pleistocene climate evolution

286

#### 287 **4.2. Late Pliocene (3.5–3.0 Ma)**

288 The new XRF data from Site 1087 confirms that the oceanographic conditions during the late  
289 Pliocene (3.5–3.0 Ma) were very different to those observed in the modern environment at this  
290 location. The high Ti counts between 3.5 and 3 Ma are associated with high alkenone MAR (this  
291 study) and a significant offset between  $U^{K}_{37'}$  and  $TEX_{86}$ -derived temperatures (Petrick et al., 2015).  
292 There is clear evidence of higher productivity, higher terrestrial input, and offsets in the different  
293 temperature proxies during the Pliocene relative to the modern, which suggests an influence of  
294 wind-driven upwelling at the site (Petrick et al., 2015a). The  $U^{K}_{37'}$  SSTs at Site 1087 were much colder  
295 than the Northern and Central Benguela Upwelling Systems (Fig. 5) (Rosell-Melé et al., 2014), but  
296 very similar to those at Site 1085 (Rommerskirchen et al., 2011). This large temperature difference  
297 between the northern/central and southern Benguela cells, over a relatively short area, is unusual in  
298 the Pliocene, where equator to pole gradients are often reduced (Fedorov et al., 2015). Rosell-Melé

299 et al. (2014) suggested the lower productivity in the northern and central cells during the Pliocene  
300 was related to overall warming in the Benguela Upwelling System, which allowed a shallow layer of  
301 warm water to restrict upwelling vigour, a phenomenon described as a “permanent Benguela Nino”  
302 (Rosell-Melé et al., 2014). Therefore, this suggests that higher productivity at Site 1087 could be  
303 related to the colder temperatures, at least during the Pliocene, although the  $U_{37}^K$ -TEX<sub>86</sub> gradient is  
304 more indicative of an increased upwelling influence in the southern Benguela region to account for  
305 enhanced productivity.

306         The XRF data indicates higher Pliocene Ti/Al values than in any other part of the record,  
307 suggesting higher terrestrial input (Figure 5). As mentioned in the intro today the site lies at the edge  
308 of both dust and riverine input pathways. Thus, the delivery pathways of terrestrial material to Site  
309 1087 must have been different during the Pliocene. We infer that this was likely related to the  
310 poleward shift in wind patterns in the Southern Hemisphere relative to today, which would have  
311 shifted dust delivery southward (Lawrence et al., 2013). Given that Ti/Al values are found to reflect  
312 dust input this is the more likely assumption (Govin et al., 2012). However, It is also possible that  
313 increased riverine input from the African continent could have increased the amount of terrestrial  
314 input reaching the cape basin, as there is some evidence that Southwest Africa was wetter during  
315 the Pliocene (Maslin et al., 2012). We unable to disentangle these two influences from the terrestrial  
316 inputs recorded here due to a lack of evidence especially other XRF record from other sites in the  
317 region, which would allow a better understating of how the terrestrial input pathways shifted during  
318 the Pliocene. However it is clear that during the Pliocene, the Benguela Upwelling System was  
319 operating differently compared to at present.

#### 320 **4.3 INHG and the early Pleistocene (3.0–1.5 Ma)**

321         Equatorward movement of the major upwelling cells may have played an important role in  
322 the transition from the warm Pliocene to colder modern temperatures around the iNHG at 2.7 Ma.  
323 (Fedorov et al., 2007). However, a closer look at data from Site 1087 suggests a more complex story

324 than the standard narrative. Changes in the size and strength of permanent upwelling in the  
325 southern Benguela Upwelling System occurred at the beginning and end of the iNHG, but not  
326 necessarily at 2.7 Ma. Between 3.0 and 2.4 Ma, when the majority North Atlantic cooling associated  
327 with iNHG occurred, the proxies at Site 1087 are stable.

328           Between 3.0 and 1.5 Ma, there is conflicting evidence about the strength of the Southern  
329 Benguela Upwelling System at Site 1087. Colder SSTs continue to be recorded at Site 1087 relative to  
330 the northern and central upwelling system (Figure 5), coupled with the continuing offset between  
331  $TEX_{86}^H$  and  $U_{37}^K$ -derived temperatures (Figure 2). Based on the recent work by Zhu et al (2016), the  
332 best explanation for the continued offset between the two temperature records is that  $TEX_{86}$  is  
333 recording conditions in shallow waters (<100 m), most likely from the centre of the upwelling region  
334 along the coast. Therefore, from the temperature proxies, it appears that water from the coastal  
335 upwelling cells was reaching Site 1087 directly across the late Pliocene-early Pleistocene. However,  
336 around 3.0 Ma, there is a decrease in primary productivity as recorded in the alkenone and chlorin  
337 MAR combined with corresponding decrease in Ti content, indicating a reduction in terrestrial input  
338 (Figures 4, 6). Thus, a clear difference emerges between the productivity data, which suggests  
339 reduced upwelling (lower productivity, less wind influence), and the temperature data, which  
340 suggests that upwelled waters continued to influence the site.

341           The differences between the productivity and temperature proxy records in upwelling  
342 systems could be explained by changes in the type of nutrients being delivered to the site, either  
343 through shifts in the local nutrient delivery paths or the nutrient content of the upwelled water  
344 (Dekens et al., 2007). The coupled decreases in Ti and productivity around 3.0 Ma suggest a  
345 connection between the loss of terrestrial input and productivity. One possibility is that a weakening  
346 or northward migration of the trade winds might have moved the major African dust plume  
347 northward (Figure 4; Etourneau et al., 2009; Martínez-García et al., 2011). It is thought that there  
348 were northward shifts in both the trade winds and westerlies during the Plio-Pleistocene transition

349 (Etourneau et al., 2010). However, most of the shifts in the wind systems occur around 2.7 Ma, after  
350 the Site 1087 Ti decreased (Etourneau et al., 2009; Lawrence et al., 2013). It is also possible the Ti  
351 decrease is related to changes in hydrology, as observed farther north at Site 1085, suggesting a  
352 drier west Africa (Maslin et al., 2012). The change in terrestrial input suggests that shifts occurred in  
353 the local wind fields and oceanic terrestrial delivery patterns around 3.0 Ma, which are likely  
354 partially related to changes in nutrient delivery to the site.

355         The low (non-diatom) productivity at Site 1087 occurs within the same time interval as the  
356 Matuyama Diatom Maximum (MDM; 3.0-2.0 Ma) in the rest of the Benguela Upwelling System  
357 (Leduc et al., 2014; Robinson and Meyers, 2002) (Figure 6). Changes in the type and amount of  
358 nutrients delivered to the upwelling zone can control the amount and type of primary productivity in  
359 the upwelling zone (Lawrence et al., 2006; März et al., 2013). The MDM, which starts around 3.0 Ma  
360 in the northern and central cells, occurs at the same time as other biogenic silica increases in other  
361 upwelling cells all over the world (März et al., 2013). Increases in the Si content of the Antarctic  
362 Intermediate Water led to increases in the amount of biogenic silica production in global upwelling  
363 cells (März et al., 2013). In the northern and central Benguela, this increase in diatom production  
364 occurs despite reduced upwelling strength (Leduc et al., 2014; Robinson and Meyers, 2002). We  
365 were unable to determine biogenic silica content at Site 1087, so we cannot consider directly the  
366 role of silicate supply on diatom production. However, the timing between the start of the MDM and  
367 the decrease in upwelling mean that it is likely increases in biogenic silica in the Antarctic  
368 Intermediate Water are responsible to the decrease in non-silica productivity in the entire Benguela  
369 Upwelling System.

370         Between 2.4–2.0 Ma,  $U^{K_{37}}$ -derived SSTs decrease at Site 1087, there was a slight increase in  
371 alkenone MARs, but no increase in chlorin MARs and no change in terrestrial inputs (Figures 2, 3,  
372 and 6). During this interval, cooling of  $U^{K_{37}}$ -derived SSTs is also observed at Site 1084 (Figure 5),  
373 accompanied by evidence of upwelling intensification (Robinson and Meyers, 2002; Rosell-Melé et

374 al., 2014), yet only alkenone MAR increases at Site 1087. Climate changes around 2.4 Ma have been  
375 previously linked to increases in the Walker circulation (Brierley and Fedorov, 2010; Liu et al., 2008;  
376 Rosell-Melé et al., 2014). The increased Walker Circulation may have increased upwelling vigour,  
377 allowing nutrients from the coastal southern upwelling cells to be delivered to Site 1087. There is an  
378 increase in alkenone productivity at Site 1087 around 2.4 Ma. Therefore it is likely, given the similar  
379 timing of temperature and productivity changes in Sites 1087 and 1084, that the increasing strength  
380 of the Walker circulation caused a northward expansion of upwelling in the Benguela Upwelling  
381 System (Etourneau et al., 2010).

382           Shifting global winds were not likely controlling the location, extent, temperature, or  
383 intensity of the southern Benguela Upwelling System when other records show major equatorward  
384 shifts in upwelling at 2.7 Ma (Lawrence et al. 2013). Instead, most of the system-wide upwelling  
385 changes seem to be driven by external shifts in the nutrients being delivered to the upwelling system  
386 from around 3.0 Ma. Instead, around 2.7 Ma the Benguela Upwelling System is responding more to  
387 local changes in nutrient supply and upwelling temperatures. This is similar to the results seen in the  
388 Peruvian Margin, where changes in the SST within the upwelling zone occurred before 2.7 Ma  
389 (Dekens et al., 2007). Given the importance of coastal upwelling to nutrient cycling and CO<sub>2</sub>  
390 exchange, data emphasize the importance of understanding the impact of nutrient changes on  
391 coastal upwelling cells.

392

#### 393 **4.4 Mid- and Late Pleistocene (1.5–0.0 Ma)**

394           Around 1.5 Ma, there is a change in the relationship between the Southern Benguela  
395 Upwelling System and the rest of the Benguela Upwelling System. SSTs decrease at Site 1087  
396 between 1.5 and 0.9 Ma (across the MPT), accompanied by increases in Ca/Ti, with a later increase  
397 in chlorin MAR from 1.5 Ma and an increase in alkenone MAR from 1.1 Ma (Figures 2; 3). The U<sup>K</sup><sub>37'</sub> -  
398 SST cooling has a global component, as it is observed in all records from the SE Atlantic Ocean.



399 However, it is 300-kyr earlier than most other basins which show cooling starting around 1.2 Ma  
400 (Figure 4; Etourneau et al., 2010; Martinez-Garcia et al., 2010; McClymont et al., 2013; Rosell-Melé  
401 et al., 2014). From 1.5 Ma, the observed increase in chlorin MAR at Site 1087 is also accompanied by  
402 increases in the alkenone MAR in the northern and central cells (Rosell-Melé et al., 2014) (Figure 6).  
403 Therefore, it appears that at 1.5 Ma, both the northern and southern Benguela Upwelling System  
404 showed similar increase in productivity, which could indicate that there had been expansion of the  
405 Benguela Upwelling System to the north. In the southern Benguela Upwelling System, the large  
406 increases in Ca/Ti values coupled with increasing alkenone MARs indicate that the central upwelling  
407 cells were moving away from Site 1087, which was now influenced instead by the edge of the  
408 upwelling zone (Giraudeau et al., 1993; Giraudeau and Rogers, 1994). This is because increased  
409 coccolithophore deposition in the Benguela Upwelling System indicates a shift towards less  
410 turbulent conditions and a more marginal upwelling setting at Site 1087 (Giraudeau et al., 1993;  
411 Giraudeau and Rogers, 1994).

412 The data also shows less primary productivity during interglacials after 0.9 Ma (Petrick et al.,  
413 2015b) (Figure 2). From 0.9 Ma onward, there is a clear shift in the SST gradient between Sites 1087  
414 and 1084, the latter of which inhabits the central upwelling cell (Figure 4), demonstrating a reduced  
415 connection between the two sites as upwelling at Site 1084 intensifies. We interpret this pattern as  
416 indicating an increasingly reduced influence of Benguela Upwelling System to Site 1087, in turn  
417 reducing the productivity at the site during the glacial terminations and interglacials since 0.9 Ma,  
418 consistent with modern oceanography (Boebel et al., 2003). However, this occurs as the northern  
419 and central upwelling cells indicate increased productivity and cooling (Rosell-Melé et al., 2014),  
420 suggesting that the modern day extent of upwelling started around 0.6 Ma (Rosell-Melé et al., 2014).  
421 This is confirmed by coeval increases in the Ca/Ti ratio at Site 1087 across the entire mid to late  
422 Pleistocene (Figure 3), which is supportive of a more marginal upwelling setting. Despite the overall  
423 trend of decreasing upwelling influence at ODP Site 1087, during the earlier 'glacial' modes of the

424 upwelling there are often short increases in upwelling strength determined by increases in chlorin  
425 MARs (Petrick et al. 2015a).

426 After 0.9 Ma, the  $TEX_{86}$  and  $U^{K}_{37'}$ -derived temperatures at Site 1087 converge and SSTs warm by 2° C  
427 between 0.6 and 0.0 Ma. This increase is superimposed upon large amplitude variations in all the  
428 proxy records (Figures 3; 4), which occur at the same time as the onset of the quasi-100-kyr glacial-  
429 interglacial cycles that mark the Early Mid-Pleistocene Transition (EMPT) (Maslin and Brierley, 2015).  
430 After the EMPT, the pattern of glacials and interglacials changes to a tripartite mode composed of an  
431 interglacial, a glacial and a full glacial (Maslin and Brierley, 2015). At ODP Site 1087 productivity  
432 decreases, and the abundance of the Agulhas Leakage indicator foraminifera, *G. menardii*, increases  
433 during the 'full glacial' portion of the deglaciation over the last 1.2 Ma (Caley et al., 2014, 2012). This  
434 is around the same time that the relationship between the various SST proxies changes and average  
435 temperatures start increasing. Furthermore previous work showed that increases in temperature at  
436 ODP 1087 had the exact same timings as temperature increases in the leakage zone proper (Caley et  
437 al., 2014, 2012; Petrick et al., 2015b). Increased Agulhas Leakage there fore might be linked to the  
438 start of the quasi-100-kyr post-EMPT cycles (Caley et al., 2014, 2012; Peeters et al., 2004). However  
439 the changes in temperature could also be linked to the previously mentioned reduction in Benguela  
440 upwelling around ODP 1087. Furthermore studies show that changes in temperature and salt  
441 leakage do not necessarily relate to changes in the amount of Auglhas leakage (Simon et al., 2015).  
442 Despite this it is clear that there is a major change of the effect of the Agulhas Leakage on the site  
443 after the EMPT in line with the other changes at that time. Therefore even if there was not any  
444 change in the location or strength of the Agulhas Leakage it is still clear that there was a major  
445 recognition of the SE Atlantic that allowed it to have a more direct impact on ODP site 1087. Future  
446 studies are needed to better understand the changes in the Auglhas leakage over the last 3.5 Ma.

## 447 **5. Conclusions**

448 New geochemical data from ODP Site 1087 reveal a complex timing of shifts in the intensity  
449 of southern Benguela Upwelling System and the initiation of increased Agulhas Leakage over the  
450 Pliocene and Pleistocene. First, records indicate that the southern Benguela Upwelling System was  
451 also influenced by the changes in nutrients and by warmer SSTs between 3.0 and 2.0 Ma. There is no  
452 evidence for a northward movement of the focus or extent of upwelling around 2.7 Ma, suggesting  
453 that changes in the wind fields had limited/no impact over the extent and strength of the upwelling  
454 during the iNHG. Finally, northward movement of the Benguela Upwelling System occurred around  
455 0.9 Ma, such that Site 1087 becomes dominated by the effects Agulhas Leakage by 0.6 Ma. This  
456 observation suggests that oceanographic changes during the MPT established the modern extent of  
457 the Benguela Upwelling System and Agulhas Leakage. Considered together, these factors  
458 demonstrate the development of the modern extent of upwelling, at least in the SE Atlantic, was  
459 complex and different from the linear northward progression that has been seen in other open  
460 ocean upwelling cells, and emphasises the importance of reconstructing information from multiple  
461 sites within an upwelling system to better understand the complete picture of upwelling  
462 development.

#### 463 **Acknowledgements.**

464 **The authors would like to thank Newcastle University and the department of Geography for**  
465 **funding this research through a School studentship. I would also like to thank the University**  
466 **college of London and University of Bristol for pervading resources as well. Additional funding**  
467 **came from Durham University and the Max Planck Society. ELM acknowledges the support of a**  
468 **Philip Leverhulme Prize. I would also like to thank IODP for providing the samples to work on and**  
469 **the MARUM in Bremen for use of the scanning XRF. I would like to thank Tomas Westerhold, and**  
470 **Jessie Farmer for their input on the data and input on the data. I would also like to thank James**  
471 **Petrick for copy editing the data. The data will be available in PANGEA on final publication.**

#### 472 **Citations**

473 Barreiro, M., Philander, G., Pacanowski, R., Fedorov, A., 2005. Simulations of warm tropical  
474 conditions with application to middle Pliocene atmospheres. *Clim. Dyn.* 26, 349–365.  
475 doi:10.1007/s00382-005-0086-4

476 Beal, L.M., De Ruijter, W.P.M., Biastoch, A., Zahn, R., 136, S.W.G., Cronin, M., Hermes, J., Lutjeharms,  
477 J., Quartly, G., Tozuka, T., Baker-Yeboah, S., Bornman, T., Cipollini, P., Dijkstra, H., Hall, I., Park,  
478 W., Peeters, F., Penven, P., Ridderinkhof, H., Zinke, J., 2011. On the role of the Agulhas system  
479 in ocean circulation and climate. *Nature* 472, 429–436. doi:10.1038/nature09983

480 Biastoch, A., Böning, C.W., Lutjeharms, J.R.E., 2008. Agulhas leakage dynamics affects decadal  
481 variability in Atlantic overturning circulation. *Nature* 456, 489–492. doi:10.1038/nature07426

482 Bluck, B.J., Ward, J.D., Cartwright, J., Swart, R., 2007. The Orange River, southern Africa: an extreme  
483 example of a wave-dominated sediment dispersal system in the South Atlantic Ocean. *J. Geol.*  
484 *Soc. London.* 164, 341–351. doi:10.1144/0016-76492005-189

485 Boebel, O., Lutjeharms, J., Schmid, C., Zenk, W., Rossby, T., Barron, C., 2003. The Cape Cauldron: a  
486 regime of turbulent inter-ocean exchange. *Deep. Res. Part II-Topical Stud. Oceanogr.* 50, 57–86.

487 Brierley, C.M., Fedorov, A. V., 2010. Relative importance of meridional and zonal sea surface  
488 temperature gradients for the onset of the ice ages and Pliocene-Pleistocene climate evolution.  
489 *Paleoceanography* 25, PA2214. doi:10.1029/2009PA001809

490 Caley, T., Giraudeau, J., Malaize, B., Rossignol, L., Pierre, C., 2012. Agulhas leakage as a key process in  
491 the modes of Quaternary climate changes. *Proc. Natl. Acad. Sci.* 109, 6835–6839.  
492 doi:10.1073/pnas.1115545109

493 Caley, T., Peeters, F.J.C., Biastoch, A., Rossignol, L., Sebille, E. Van, 2014. *Geophysical Research*  
494 *Letters* 1238–1246. doi:10.1002/2014GL059278. Received

495 Chalk, T.B., Hain, M.P., Foster, G.L., Rohling, E.J., Sexton, P.F., Badger, M.P.S., Cherry, S.G.,  
496 Hasenfratz, A.P., Haug, G.H., Jaccard, S.L., Martínez-García, A., Pälike, H., Pancost, R.D., Wilson,  
497 P.A., 2017. Causes of ice age intensification across the Mid-Pleistocene Transition. *Proc. Natl.*  
498 *Acad. Sci.* 114, 201702143. doi:10.1073/pnas.1702143114

499 Christensen, B.A., Giraudeau, J., 2002. Neogene and Quaternary evolution of the Benguela upwelling  
500 system - Foreword. *Mar. Geol.* 180, 1–2.

501 Compton, J., Herbert, C., Schneider, R., 2009. Organic-rich mud on the western margin of southern  
502 Africa: Nutrient source to the Southern Ocean? *Glob. Biogeochem. Cycles* 23, GB4030.  
503 doi:10.1029/2008gb003427

504 Compton, J.S., Maake, L., 2007. Source of the suspended load of the upper Orange River, South  
505 Africa. *South African J. Geol.* 110, 339–348. doi:10.2113/gssajg.110.2-3.339

506 Dekens, P.S., Ravelo, A.C., McCarthy, M.D., 2007. Warm upwelling regions in the Pliocene warm  
507 period. *Paleoceanography* 22, PA3211. doi:10.1029/2006pa001394

508 Diester-Haass, L., 1988. Sea level changes, carbonate dissolution and history of the Benguela Current  
509 in the Oligocene-Miocene off Southwest Africa (DSDP Site 362, Leg 40). *Mar. Geol.* 79, 213–  
510 242. doi:10.1016/0025-3227(88)90040-0

511 Dyez, K.A., Zahn, R., Hall, I.R., 2014. Multicentennial Agulhas leakage variability and links to North  
512 Atlantic climate during the past 80,000 years. *Paleoceanography* 29, 1238–1248.  
513 doi:10.1002/2014PA002698

514 Etourneau, J., Martinez, P., Blanz, T., Schneider, R., 2009. Pliocene-Pleistocene variability of  
515 upwelling activity, productivity, and nutrient cycling in the Benguela region. *Geology* 37, 871–  
516 874. doi:10.1130/G25733A.1

517 Etourneau, J., Schneider, R., Blanz, T., Martinez, P., 2010. Intensification of the Walker and Hadley  
518 atmospheric circulations during the Pliocene-Pleistocene climate transition. *Earth Planet. Sci.*

519 Lett. 297, 103–110. doi:10.1016/j.epsl.2010.06.010

520 Fedorov, A., Barreiro, M., Boccaletti, G., Pacanowski, R., Philander, S.G., 2007. The Freshening of  
521 Surface Waters in High Latitudes: Effects on the Thermohaline and Wind-Driven Circulations. *J.*  
522 *Phys. Oceanogr.* 37, 896–907. doi:10.1175/jpo3033.1

523 Fedorov, A. V., Burls, N.J., Lawrence, K.T., Peterson, L.C., 2015. Tightly linked zonal and meridional  
524 sea surface temperature gradients over the past five million years. *Nat. Geosci.* 8, 975–980.  
525 doi:10.1038/ngeo2577

526 Giraudeau, J., Monteiro, P.M.S., Nikodemus, K., 1993. Distribution and malformation of living  
527 coccolithophores in the northern Benguela upwelling system off Namibia. *Mar. Micropaleontol.*  
528 22, 93–110. doi:10.1016/0377-8398(93)90005-I

529 Giraudeau, J., Rogers, J., 1994. Phytoplankton Biomass and Sea-Surface Temperature Estimates from  
530 Sea-Bed Distribution of Nannofossils and Planktonic Foraminifera in the Benguela Upwelling  
531 System. *Micropaleontology* 40, 275. doi:10.2307/1485822

532 Gordon, A.L., Haxby, W.F., 1990. Agulhas Eddies Invade the South Atlantic: Evidence From Geosat  
533 Altimeter and Shipboard Conductivity-Temperature-Depth Survey. *J. Geophys. Res.* 95, 3117–  
534 3125. doi:10.1029/JC095iC03p03117

535 Gordon, A.L., Lutjeharms, J.R.E., Gründlingh, M.L., 1987. Stratification and circulation at the Agulhas  
536 Retroflection. *Deep Sea Res. Part A. Oceanogr. Res. Pap.* 34, 565–599.

537 Govin, A., Holzwarth, U., Heslop, D., Ford Keeling, L., Zabel, M., Mulitza, S., Collins, J.A., Chiessi, C.M.,  
538 2012. Distribution of major elements in Atlantic surface sediments (36°N–49°S): Imprint of  
539 terrigenous input and continental weathering. *Geochemistry, Geophys. Geosystems* 13, n/a-  
540 n/a. doi:10.1029/2011GC003785

541 Hall, C., Lutjeharms, J.R.E., 2011. Cyclonic eddies identified in the Cape Basin of the South Atlantic  
542 Ocean. *J. Mar. Syst.* 85, 1–10.

543 Harris, P.G., Zhao, M., Rosell-Mele, A., Tiedemann, R., Sarnthein, M., Maxwell, J.R., 1996. Chlorin  
544 accumulation rate as a proxy for Quaternary marine primary productivity. *Nature* 383, 63–65.

545 Haug, G.H., Ganopolski, A., Sigman, D.M., Rosell-Mele, A., Swann, G.E.A., Tiedemann, R., Jaccard,  
546 S.L., Bollmann, J., Maslin, M.A., Leng, M.J., Eglinton, G., 2005. North Pacific seasonality and the  
547 glaciation of North America 2.7 million years ago. *Nature* 433, 821–825.  
548 doi:10.1038/nature03332

549 Jung, G., Prange, M., Schulz, M., 2014. Uplift of Africa as a potential cause for Neogene  
550 intensification of the Benguela upwelling system. *Nat. Geosci. advance on*, 741–747.  
551 doi:10.1038/ngeo2249

552 Kienast, S.S., Winckler, G., Lippold, J., Albani, S., Mahowald, N.M., 2016. Tracing dust input to the  
553 global ocean using thorium isotopes in marine sediments: ThoroMap. *Global Biogeochem.*  
554 *Cycles* 30, 1526–1541. doi:10.1002/2016GB005408

555 Knorr, G., Lohmann, G., 2003. Southern Ocean origin for the resumption of Atlantic thermohaline  
556 circulation during deglaciation. *Nature* 424, 532–536. doi:10.1038/nature01855

557 Kornilova, O., Rosell-Mele, A., 2003. Application of microwave-assisted extraction to the analysis of  
558 biomarker climate proxies in marine sediments. *Org. Geochem.* 34, 1517–1523.  
559 doi:10.1016/s0146-6380(03)00155-4

560 Lawrence, K.T., Liu, Z., Herbert, T.D., 2006. Evolution of the eastern tropical Pacific through Plio-  
561 Pleistocene glaciation. *Science* 312, 79–83. doi:10.1126/science.1120395

562 Lawrence, K.T., Sigman, D.M., Herbert, T.D., Riihimaki, C.A., Bolton, C.T., Martinez-Garcia, A., Rosell-  
563 Mele, A., Haug, G.H., 2013. Time-transgressive North Atlantic productivity changes upon  
564 Northern Hemisphere glaciation. *Paleoceanography* 28, 740–751. doi:10.1002/2013PA002546

565 Leduc, G., Garbe-Schönberg, D., Regenberg, M., Contoux, C., Etourneau, J., Schneider, R., 2014. The  
566 late Pliocene Benguela upwelling status revisited by means of multiple temperature proxies.  
567 *Geochemistry, Geophys. Geosystems* 15, 475–491. doi:10.1002/2013GC004940

568 Liu, Z.H., Altabet, M.A., Herbert, T.D., 2008. Plio-Pleistocene denitrification in the eastern tropical  
569 North Pacific: Intensification at 2.1 Ma. *Geochemistry Geophys. Geosystems* 9, 14.  
570 doi:10.1029/2008GC002044

571 Mahowald, N., Albani, S., Kok, J.F., Engelstaeder, S., Scanza, R., Ward, D.S., Flanner, M.G., 2014. The  
572 size distribution of desert dust aerosols and its impact on the Earth system. *Aeolian Res.* 15,  
573 53–71. doi:10.1016/J.AEOLIA.2013.09.002

574 Marino, G., Zahn, R., Ziegler, M., Purcell, C., Knorr, G., Hall, I.R., Ziveri, P., Elderfield, H., 2013.  
575 Agulhas salt-leakage oscillations during abrupt climate changes of the Late Pleistocene.  
576 *Paleoceanography* 28, 599–606. doi:10.1002/palo.20038

577 Marlow, J.R., Lange, C.B., Wefer, G., Rosell-Mele, A., 2000. Upwelling intensification as part of the  
578 Pliocene-Pleistocene climate transition. *Science (80- )*. 290, 2288–+.

579 Martínez-García, A., Rosell-Melé, A., Jaccard, S.L., Geibert, W., Sigman, D.M., Haug, G.H., Martínez-  
580 García, A., Rosell-Mele, A., Jaccard, S.L., Geibert, W., Sigman, D.M., Haug, G.H., 2011. Southern  
581 Ocean dust–climate coupling over the past four million years. *Nature* 476, 312–315.  
582 doi:10.1038/nature10310

583 Martínez-García, A., Rosell-Mele, A., McClymont, E.L., Gersonde, R., Haug, G.H., 2010. Subpolar Link  
584 to the Emergence of the Modern Equatorial Pacific Cold Tongue. *Science (80- )*. 328, 1550–  
585 1553. doi:10.1126/science.1184480

586 März, C., Schnetger, B., Brumsack, H.-J., 2013. Nutrient leakage from the North Pacific to the Bering  
587 Sea (IODP Site U1341) following the onset of Northern Hemispheric Glaciation?  
588 *Paleoceanography* 28, 68–78. doi:10.1002/palo.20011

589 Maslin, M.A., Brierley, C.M., 2015. The role of orbital forcing in the Early Middle Pleistocene  
590 Transition. *Quat. Int.* 389, 47–55. doi:10.1016/j.quaint.2015.01.047

591 Maslin, M.A., Pancost, R.D., Wilson, K.E., Lewis, J., Trauth, M.H., 2012. Three and half million year  
592 history of moisture availability of South West Africa: Evidence from ODP site 1085 biomarker  
593 records. *Palaeogeogr. Palaeoclimatol. Palaeoecol.* 317–318, 41–47.  
594 doi:10.1016/j.palaeo.2011.12.009

595 McClymont, E.L., Rosell-Melé, A., Giraudeau, J., Pierre, C., Lloyd, J.M., 2005. Alkenone and coccolith  
596 records of the mid-Pleistocene in the south-east Atlantic: Implications for the U37K' index and  
597 South African climate. *Quat. Sci. Rev.* 24, 1559–1572. doi:10.1016/j.quascirev.2004.06.024

598 McClymont, E.L., Sostdian, S.M., Rosell-Melé, A., Rosenthal, Y., 2013. Pleistocene sea-surface  
599 temperature evolution: Early cooling, delayed glacial intensification, and implications for the  
600 mid-Pleistocene climate transition. *Earth-Science Rev.* 123, 173–193.  
601 doi:10.1016/j.earscirev.2013.04.006

602 Müller, P.J., Kirst, G., Ruhland, G., von Storch, I., Rosell-Mele, A., 1998. Calibration of the alkenone  
603 paleotemperature index U-37(K') based on core-tops from the eastern South Atlantic and the  
604 global ocean (60 degrees N-60 degrees S). *Geochim. Cosmochim. Acta* 62, 1757–1772.

605 Peeters, F.J.C., Acheson, R., Brummer, G.-J.A., de Ruijter, W.P.M., Schneider, R.R., Ganssen, G.M.,  
606 Ufkes, E., Kroon, D., 2004. Vigorous exchange between the Indian and Atlantic oceans at the  
607 end of the past five glacial periods. *Nature* 430, 661–665.

608 Petrick, B., McClymont, E.L.E.L., Felder, S., Rueda, G., Leng, M.J.M.J., Rosell-Melé, A., 2015. Late  
609 Pliocene upwelling in the Southern Benguela region. *Palaeogeogr. Palaeoclimatol. Palaeoecol.*  
610 429, 62–71. doi:10.1016/j.palaeo.2015.03.042

611 Petrick, B.F., McClymont, E.L., Marret, F., Van Der Meer, M.T.J., 2015. Changing surface water  
612 conditions for the last 500 ka in the Southeast Atlantic: Implications for variable influences of  
613 Agulhas leakage and Benguela upwelling. *Paleoceanography* In revisio, 1153–1167.  
614 doi:10.1002/2015PA002787

615 Prah, F.G., Wakeham, S.G., 1987. Calibration of unsaturation patterns in long-chain ketone  
616 compositions for palaeotemperature assessment. *Nature* 330, 367–369.

617 Robinson, R.S., Meyers, P.A., 2002. Biogeochemical changes within the Benguela Current upwelling  
618 system during the Matuyama Diatom Maximum: Nitrogen isotope evidence from Ocean Drilling  
619 Program Sites 1082 and 1084. *Paleoceanography* 17, 16-1-16–10. doi:10.1029/2001pa000659

620 Rommerskirchen, F., Condon, T., Mollenhauer, G., Dupont, L., Schefuss, E., 2011. Miocene to  
621 Pliocene development of surface and subsurface temperatures in the Benguela Current system.  
622 *Paleoceanography* 26, 15. doi:Pa321610.1029/2010pa002074

623 Rosell-Melé, A., Martínez-García, A., McClymont, E.L., 2014. Persistent warmth across the Benguela  
624 upwelling system during the Pliocene epoch. *Earth Planet. Sci. Lett.* 386, 10–20.  
625 doi:10.1016/j.epsl.2013.10.041

626 Schouten, S., Hopmans, E.C., Schefuss, E., Damste, J.S.S., 2002. Distributional variations in marine  
627 crenarchaeotal membrane lipids: a new tool for reconstructing ancient sea water  
628 temperatures? (vol 204, pg 265, 2002). *Earth Planet. Sci. Lett.* 204, 265–274.

629 Scussolini, P., Marino, G., Brummer, G.-J.A.G.-J.A., Peeters, F.J.C.C., 2015. Saline Indian Ocean waters  
630 invaded the South Atlantic thermocline during glacial termination II. *Geology* 43, 139–142.  
631 doi:10.1130/G36238.1

632 Shipboard Scientific Party, 1998. Site 1087, in: Wefer Berger, W.H., Richter, C., et al., G. (Ed.), Proc.  
633 ODP, Init. Repts. Ocean Drilling Program, College Station, TX, pp. 457–484.

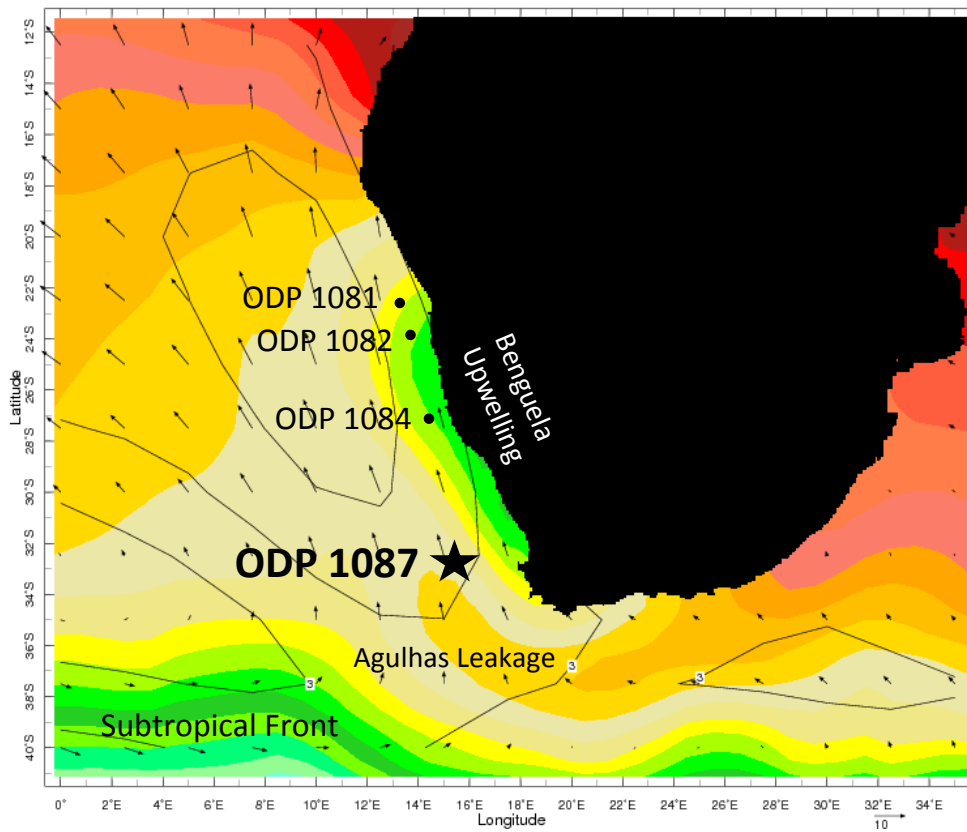
634 Simon, M.H., Gong, X., Hall, I.R., Ziegler, M., Barker, S., Knorr, G., van der Meer, M.T.J., Kasper, S.,  
635 Schouten, S., 2015. Salt exchange in the Indian-Atlantic Ocean Gateway since the Last Glacial  
636 Maximum: A compensating effect between Agulhas Current changes and salinity variations?  
637 *Paleoceanography* 30, 1318–1327. doi:10.1002/2015PA002842

638 West, S., Jansen, J.H.F., Stuut, J.B., 2004. Surface water conditions in the Northern Benguela Region  
639 (SE Atlantic) during the last 450 ky reconstructed from assemblages of planktonic foraminifera.  
640 *Mar. Micropaleontol.* 51, 321–344. doi:http://dx.doi.org/10.1016/j.marmicro.2004.01.004

641 Zachos, J.C., Kroon, D., Blum, P., 2004. Shipboard Scientific Party 2 208.

642

Time Mar 2007 Pressure 1000.0 mb



643

644

645

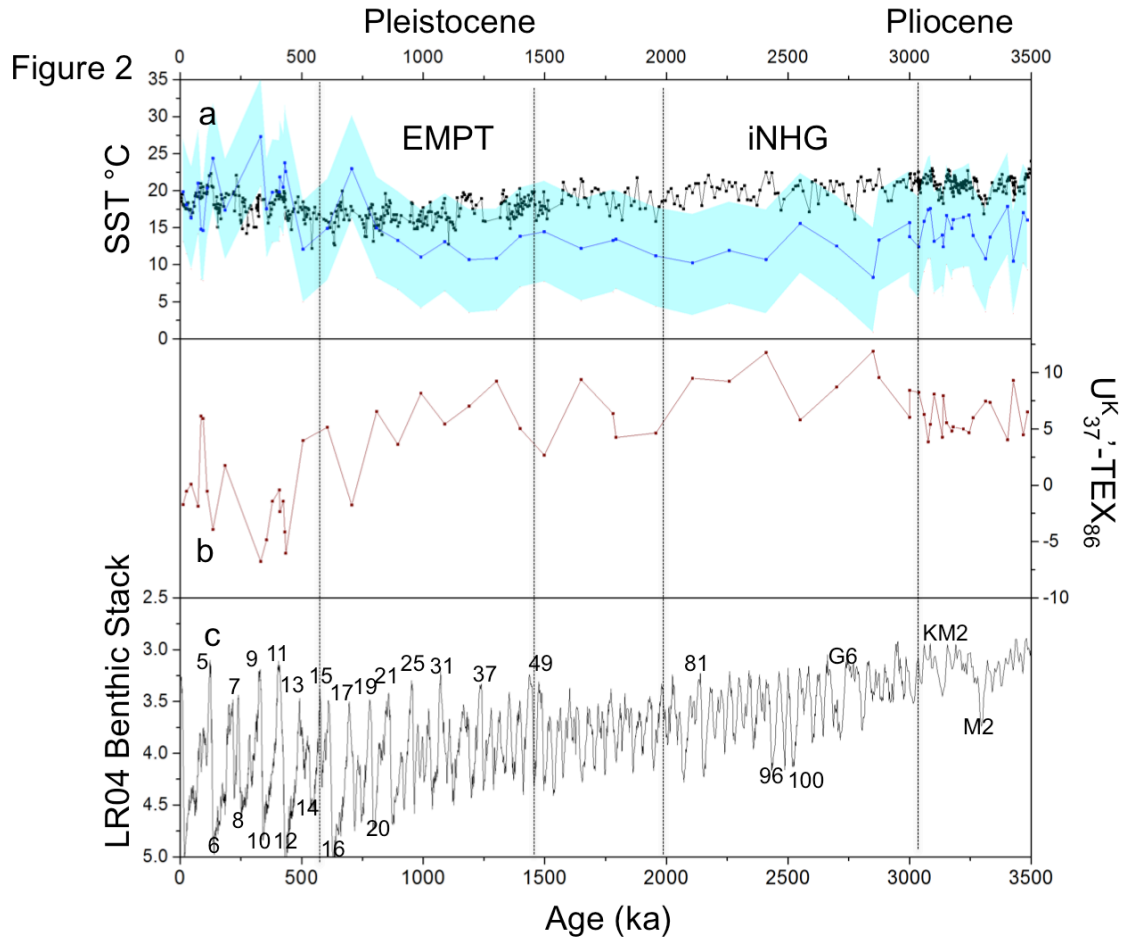
646

647

648

Figure 1: SE Atlantic map and relevant ODP drilling sites on a SST record from XXXX. Also shown are wind direction and pressure bars . The location of complementary records from this region referenced in the paper and the location of major oceanic systems in their modern day positions are shown.

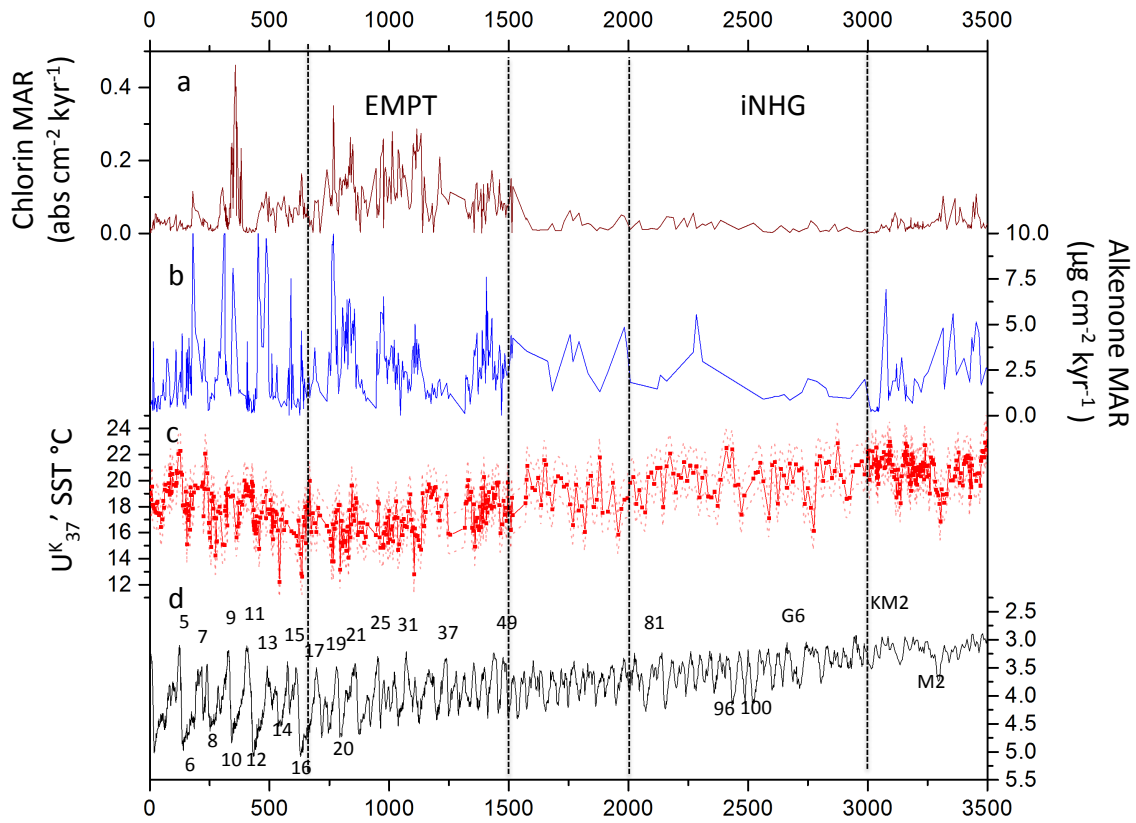




649

650 Figure 2: Temperature proxies for ODP Site 1087: a) sea surface temperature estimates derived  
 651 from  $U^{K_{37'}}$  (black line) and  $TEX_{86}$  BAYSPAR (blue line with dots) with analytical + calibration error  
 652 envelope (blue envelope); b) Difference between  $U^{K_{37'}}$  and  $TEX_{86}$  BAYSPAR derived SST estimates;  
 653 c) LR04 benthic oxygen isotope stack (Lisiecki and Raymo, 2005) with selected MIS shown. Also  
 654 major transitions in the ODP site 1087 record are showed with dashed lines and the timings of the  
 655 iNHG and EMPT are labelled.

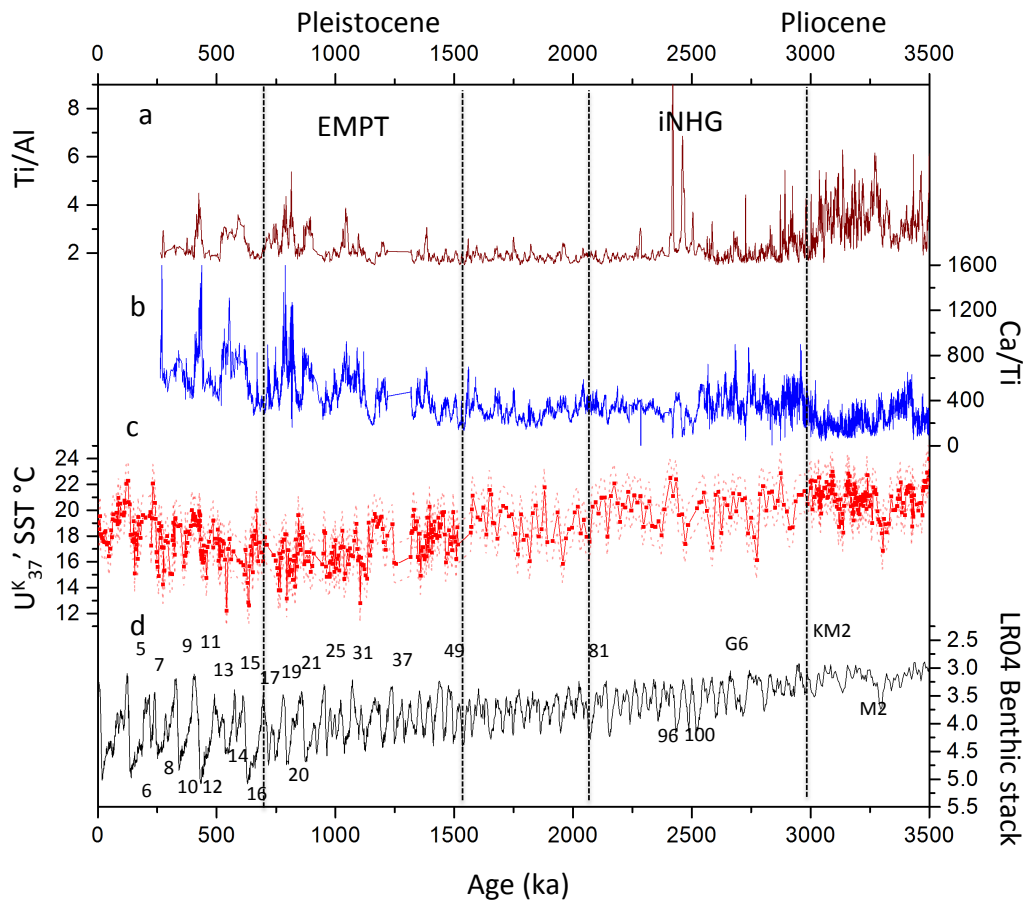
656



657

658 Figure 3: Productivity and temperature trends from ODP Site 1087: a) chlorin MARs; b) alkenone  
 659 MARs; c)  $U_{37}'$ -derived SSTs with error envelope; d) LR04 benthic oxygen isotope stack (Lisiecki and  
 660 Raymo, 2005) with selected MIS shown. The vertical dashed lines indicate the major transitions  
 661 observed in the data in terms of temperature and productivity. Also major transitions in the ODP  
 662 site 1087 record are shown with dashed lines and the timings of the iNHG and EMPT are labeled.

663



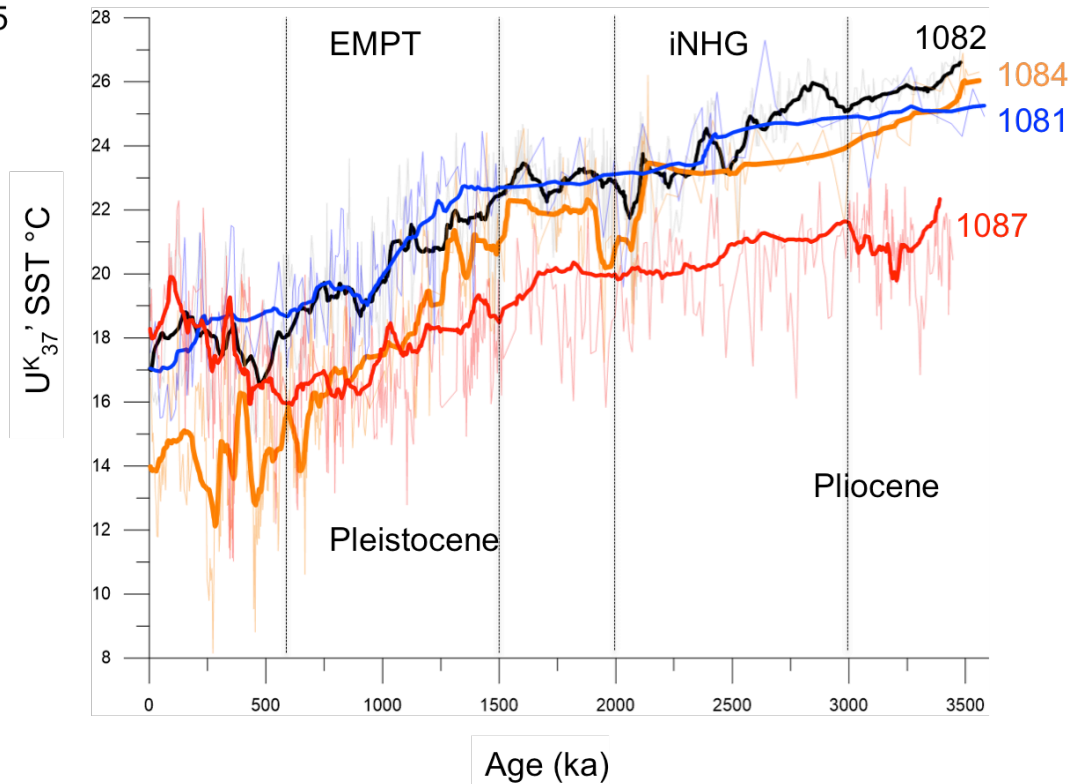
664

665 Figure 4: XRF data and temperature from ODP Site 1087: a) Ti raw counts generated by scanning  
 666 XRF; b) Ca/Ti data; c)  $U^{K}_{37}$ -derived SSTs, with error envelope includes analytical plus calibration  
 667 error; d) LR04 benthic oxygen isotope stack (Lisiecki and Raymo, 2005) with selected MIS shown.  
 668 Major transitions in the ODP site 1087 record are shown with dashed lines and the timings of the  
 669 iNHG and EMPT are labelled

670

671

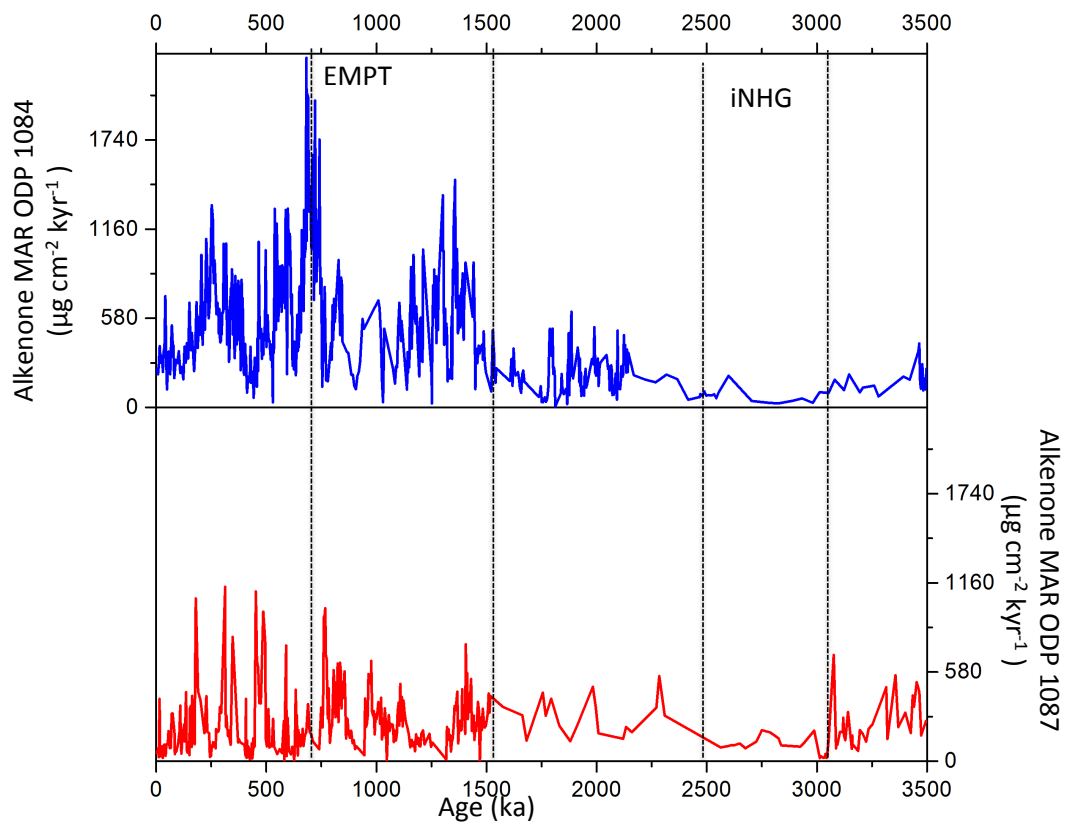
Figure 5



672

673 Figure 5: Regional SST trends. Comparing the ODP Site 1087 U<sup>K</sup><sub>37</sub>'-derived SST record (Red) to the  
674 three other Benguela Upwelling SST records: ODP Sites 1081 (brown), Site 1082 (orange), and Site  
675 1084 (blue). The dark lines for each record represent 30 point running averages. Also major  
676 transitions in the ODP site 1087 record are shown with dashed lines and the timings of the iNHG and  
677 EMPT are labelled

678



679

680 Figure 6: Alkenone MAR records from the Benguela Upwelling system over the Plio-Pleistocene:  
 681 southern cells, ODP Site 1087 (red); central cells, ODP Site 1084 Blue. Both graphs are on the same  
 682 scale so that a straight comparison of the two records can be done. Also major transitions in the  
 683 ODP site 1087 record are shown with dashed lines and the timings of the iNHG and EMPT are  
 684 labelled

685

686